1-1-2009

Effects of the surrounding medium on the optical properties of a subwavelength aperture

Olena Lopatiuk-Tirpak
University of Central Florida

Sasan Fathpour
University of Central Florida

Effects of the surrounding medium on the optical properties of a subwavelength aperture

Olena Lopatiuk-Tirpak* and Sasan Fathpour

CREOL, The College of Optics and Photonics, University of Central Florida, Orlando, FL 32816, U.S.A.
**otirpak@creol.ucf.edu*

Abstract: Influence of the refractive index of the surrounding material on the performance of a C-shaped subwavelength aperture is investigated. The changes in the spectral response (0.6 μm to 6 μm wavelength range) and power throughput of the aperture in an optically opaque silver (Ag) film are described for two configurations: one where the film with the aperture is immersed in an infinite dielectric slab and the other where the metallic layer is immediately adjacent to a semi-infinite dielectric substrate. It is shown that, while the resonant wavelengths increase monotonically with refractive index for both cases, the rates of these increases, as well as the behavior of the power throughput, depend not only on the configuration, but also strongly on the transmission mode. These findings have important implications for the design of subwavelength aperture-enhanced devices.

OCIS codes: (260.3910) Metal optics; (240.6680) Surface plasmons; (250.5403) Plasmonics; (160.4760) Optical properties; (260.2710) Inhomogeneous optical media.

References and Links

1. T. W. Ebbesen, H. J. Lezec, H. F. Ghaemi, T. Thio, and P. A. Wolff, "Extraordinary optical transmission through sub-wavelength hole arrays," Nature **391**(6668), 667–669 (1998).
2. L. Tang, D. A. B. Miller, A. K. Okyay, J. A. Matteo, Y. Yuen, K. C. Saraswat, and L. Hesselink, "C-shaped nanoaperture-enhanced germanium photodetector," Opt. Lett. **31**(10), 1519–1521 (2006).
3. L. Tang, S. Latif, and D. A. B. Miller, "Plasmonic device in silicon CMOS," Electron. Lett. **45**(13), 706 (2009).
4. S. I. Bozhevolnyi, V. S. Volkov, E. Devaux, and T. W. Ebbesen, "Channel plasmon-polariton guiding by subwavelength metal grooves," Phys. Rev. Lett. **95**(4), 046802 (2005).
5. E. C. Kinzel, and X. F. Xu, "High efficiency excitation of plasmonic waveguides with vertically integrated resonant bowtie apertures," Opt. Express **17**(10), 8036–8045 (2009).
6. R. Gordon, D. Sinton, K. L. Kavanagh, and A. G. Brolo, "A new generation of sensors based on extraordinary optical transmission," Acc. Chem. Res. **41**(8), 1049–1057 (2008).
7. A. Krishnan, T. Thio, T. J. Kima, H. J. Lezec, T. W. Ebbesen, P. A. Wolff, J. Pendry, L. Martin-Moreno, and F. J. Garcia-Vidal, "Evanescently coupled resonance in surface plasmon enhanced transmission," Opt. Commun. **200**(1-6), 1–7 (2001).
8. J. J. Mock, D. R. Smith, and S. Schultz, "Local refractive index dependence of plasmon resonance spectra from individual nanoparticles," Nano Lett. **3**(4), 485–491 (2003).
9. M. H. Lee, H. W. Gao, and T. W. Odom, "Refractive index sensing using quasi one-dimensional nanoslit arrays," Nano Lett. **9**(7), 2584–2588 (2009).
10. H. Guo, T. P. Meyrath, T. Zentgraf, N. Liu, L. Fu, H. Schweizer, and H. Giessen, "Optical resonances of bowtie slot antennas and their geometry and material dependence," Opt. Express **16**(11), 7756–7766 (2008).
11. X. L. Shi, and L. Hesselink, "Design of a C aperture to achieve λ/10 resolution and resonant transmission," J. Opt. Soc. Am. B **21**(7), 1305–1317 (2004).
12. X. L. Shi, and L. Hesselink, "Mechanisms for enhancing power throughput from planar nano-apertures for near-field optical data storage," Jpn. J. Appl. Phys. **41**(Part 1, No. 3B), 1632–1635 (2002).
13. Z. F. Yu, G. Veronis, S. H. Fan, and M. L. Brongersma, "Design of midinfrared photodetectors enhanced by surface plasmons on grating structures," Appl. Phys. Lett. **89**(15), 151116 (2006).
14. P. Hansen, L. Hesselink, and B. Leen, "Design of a subwavelength bent C-aperture waveguide," Opt. Lett. **32**(12), 1737–1739 (2007).
15. L. Y. Sun, and L. Hesselink, "Low-loss subwavelength metal C-aperture waveguide," Opt. Lett. **31**(24), 3606–3608 (2006).
16. Z. L. Rao, J. A. Matteo, L. Hesselink, and J. S. Harris, "High-intensity C-shaped nanoaperture vertical-cavity surface-emitting laser with controlled polarization," Appl. Phys. Lett. **90**(19), 191110 (2007).

#120095 - $15.00 USD Received 17 Nov 2009; revised 8 Dec 2009; accepted 10 Dec 2009; published 14 Dec 2009

17. J. W. Lee, M. A. Seo, D. S. Kim, J. H. Kang, and Q. H. Park, "Polarization dependent transmission through asymmetric C-shaped holes," Appl. Phys. Lett. **94**(8), 081102–081103 (2009).
18. B. A. Munk, Frequency selective surfaces: theory and design (John Wiley & Sons, New York, 2000).
19. H. Shin, P. B. Catrysse, and S. Fan, "Effect of the plasmonic dispersion relation on the transmission properties of subwavelength cylindrical holes," Phys. Rev. B **72**(8), 085436 (2005).
20. M. A. Ordal, L. L. Long, R. J. Bell, S. E. Bell, R. R. Bell, R. W. Alexander, Jr., and C. A. Ward, "Optical properties of the metals Al, Co, Cu, Au, Fe, Pb, Ni, Pd, Pt, Ag, Ti, and W in the infrared and far infrared," Appl. Opt. **22**(7), 1099–1119 (1983).
21. J. Matteo, and L. Hesselink, "Fractal extensions of near-field aperture shapes for enhanced transmission and resolution," Opt. Express **13**(2), 636–647 (2005).
22. Y. Pang, C. Genet, and T. W. Ebbesen, "Optical transmission through subwavelength slit apertures in metallic films," Opt. Commun. **280**(1), 10–15 (2007).

1. Introduction

Subwavelength apertures have been the subject of many computational and experimental investigations ever since the demonstration of the extraordinary optical transmission [1]. The ability to combine high irradiance with subwavelength spot size opens the door to many new applications, including high-speed, high-responsivity photodetectors [2,3], nanophotonic circuits [4,5], and chemical and biological sensors [6].

While several earlier works have addressed the role of the surrounding medium in subwavelength metal optics [7–9], most studies of subwavelength apertures are performed on free-standing metal films [10–12] or films on a dielectric with a constant refractive index, n [13]. This work will show that there are substantial qualitative and quantitative differences between these two cases, which ought to be accounted for in device design. A single C-shaped subwavelength aperture is chosen for this systematic study. The chief advantage of the C-shaped antenna over aperture arrays and corrugation-enhanced apertures is in its compact size [2], which renders it better suited for nanophotonic applications. Promising implementation of C-shaped antennas has been proposed and/or implemented for photodetectors [2,3], waveguides [14,15], surface-emitting lasers [16], and switchable transmission filters [17].

It is widely accepted that the resonant wavelength of a frequency-selective metallic surface structure embedded in an infinite dielectric medium scales linearly with the refractive index of the latter, n [18]. Similarly, a $\sqrt{(n^2+1)/2}$ scaling [18] is commonly argued to be applicable to metallic layers on a semi-infinite substrate. These approximations are often cited to predict the substrate effects on the optical properties [10,19]. However, results reported below show that while the scaling holds true for immersed apertures, the more realistic configuration, i.e., when the aperture is fabricated in a plasmonic metal (as opposed to perfect electric conductor) on a dielectric substrate, presents itself with many consequential, qualitative and quantitative differences. In this case, the extent and the manner in which resonant wavelengths and the power throughput vary with n depend on the specific transmission mechanism involved. Understanding these differences is critical for successful design and accurate performance predictions of aperture-enhanced plasmonic devices. To the best of the authors' knowledge, this is the first systematic computational study of an aperture with plasmonic metals on dielectric substrates under the conditions of varying n of the surrounding medium.

2. Methodology

The dimensions of the aperture used in this work are shown in Fig. 1(a). The shape of the aperture was borrowed from our initial studies (not presented here) that aimed at maximizing the power throughput (PT) at near-IR wavelengths. To illuminate the nature of the transmission modes, the Ag layer thickness, d, was varied from 100 to 1000 nm. For varying refractive index studies, d was chosen to be 300 nm, for reasons that will be presented in context below. The calculations were performed using the finite-integration method within the CST Microwave Suite. Optical properties of the Ag were simulated by fitting the experimentally obtained dielectric constant values [20] to the Drude model in the wavelength

#120095 - $15.00 USD Received 17 Nov 2009; revised 8 Dec 2009; accepted 10 Dec 2009; published 14 Dec 2009

range of 0.6 μm to 6 μm. Silver was chosen over other commonly used metals, such as gold or aluminum, because of its low absorption losses (imaginary dielectric constant) in the studied spectral range. The material surrounding the aperture is modeled as a lossless dielectric. The excitation source was a plane wave with the amplitude of 1 V/m, polarized along the *x*-axis. Absorbing boundary conditions were set for all six boundaries.

In order to determine the spectral characteristics of the aperture response, the excitation was delivered as a pulse with the duration of ~5 femtoseconds, roughly covering the mentioned 0.6 μm to 6 μm wavelength range. The spectral response was assumed to be represented by the local electric field at the point P1 [Fig. 1(a)], located at the exit surface. This assumption was verified at several other points on the exit surface, where despite the relative intensity variations, the major spectral features were found to remain unchanged.

The fraction of energy transmitted by the aperture was quantified by calculating the PT [21] at a wavelength of interest. PT is defined as the ratio of total exit power surface to that impinging upon the physical area of the aperture and was calculated by integrating the normal component of the Poynting vector over the entire surface of the aperture in the plane immediately adjacent to the Ag layer. It should be clarified that because near-field radiation, in general, contains both propagating and evanescent components, the values of PT may change with distance from the exit surface. Therefore, PT should be viewed as a metric for comparison, rather than a quantitative measure of extraordinary transmittance.

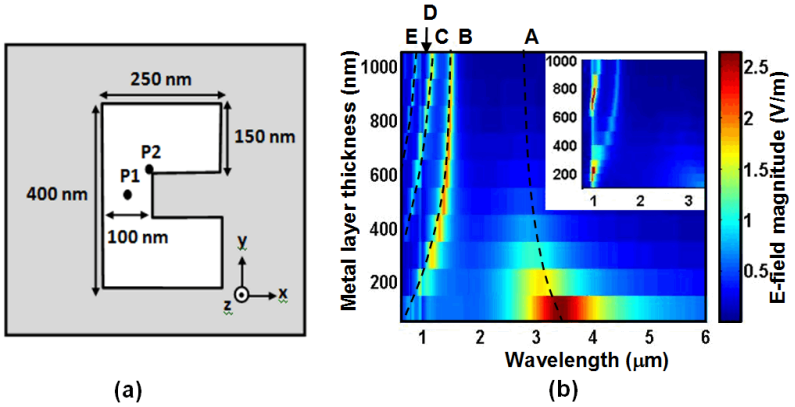

Fig. 1. (a) The schematic representation of the studied aperture, showing the location of the *E*-field probes used to evaluate the spectral response. The excitation radiation propagates in the $-z$ direction; (b) Evolution of the *E*-field spectral response with increasing *d*, measured at point P1 in Fig. 1(a) and for the case of aperture on a dielectric substrate with $n = 3.45$. Inset: Spectral response as a function of thickness at point P2 in Fig. 1(a). The color scale of the inset is 10 times that of the main figure.

3. Results and discussion

Before discussing the role of the surrounding material, it is helpful to examine the different transmission mechanisms of the C-shaped aperture. The origin of the transmittance peaks in the spectral response can be deduced by monitoring the shifts of the resonant wavelengths while changing the thickness of the metal layer. The evolution of the response with *d* is shown in Fig. 1(b) as an example of the aperture-on-substrate configuration, where the Ag film is immediately adjacent to a substrate with $n = 3.45$ (that of silicon), and the remainder of the space, including the aperture cavity, is set to $n = 1$. The response is measured at point P1 in Fig. 1(a), and the excitation impinges on the system from the vacuum side. In the studied wavelength range, the response shows the evolution of several peaks: one that undergoes a blue shift with increasing *d* (peak A), three that red-shift (peaks B, C, and E), and a faint thickness-invariant peak denoted as D.

#120095 - $15.00 USD Received 17 Nov 2009; revised 8 Dec 2009; accepted 10 Dec 2009; published 14 Dec 2009

Peak A is present even for infinitesimally thin metal layer (the thickness of one mesh cell, not shown) and is most likely caused by the interaction of two evanescent surface waves on either side of the aperture [7]. In other words, the surface plasmons excited by the incident pulse on each metal-dielectric interface couple to each other inside the aperture cavity with a strength that is chiefly determined by how well-matched their frequencies are. As confirmed below, the transmittance through the aperture is highest when the refractive indices of the front and back materials are the same, as this allows for constructive interference of the evanescent waves inside the aperture. On the other hand, for the case presented in Fig. 1(b), where the index of the substrate differs substantially from that of the entrance surface, the plasmon frequencies differ significantly, resulting in weak coupling; this in turn causes the transmittance to decrease rapidly with increasing thickness. From here on, this mode will be referred to as the evanescently coupled surface plasmon (ECSP) mode.

Peaks B, C, and E correspond to the different orders of a Fabry-Perot-like (FP) aperture cavity mode, as suggested by their thickness dependence and by the electric field (*E*-field) profiles taken at the corresponding wavelengths (Fig. 2). The wavelength, λ, of the FP resonances is determined not only by the cavity thickness, but also by the phase change, ϕ, upon reflection from the front and back surfaces: $\lambda = 2d / (N - \varphi / \pi)$, where N is an integer. Therefore, the spectral position of the FP peaks can differ considerably from $2d/N$ [22].

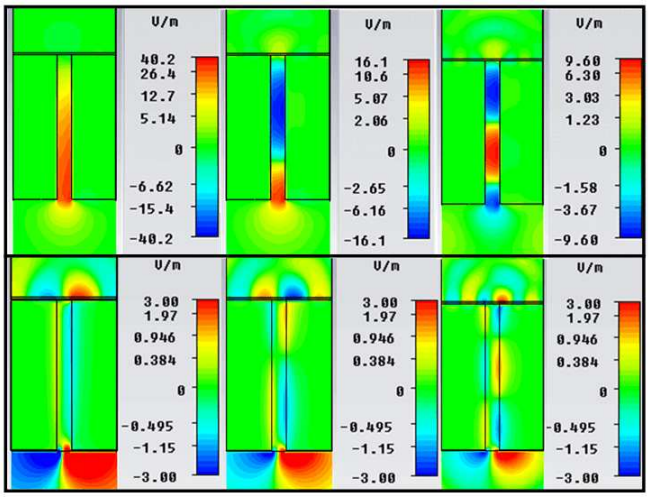

Fig. 2. *E*-field distributions for d = 1000 nm at the wavelengths of the FP modes (random phase). The wavelengths are, from left to right: 1.51 μm, 1.16 μm, and 875 nm, corresponding to peaks B, C and E in Fig. 1(b), respectively. The *x*- and z-component are shown in the top and bottom panels, respectively. The plane shown corresponds to the *x*-*z* plane containing the point P1 of Fig. 1(a).

The peak D has a signature of a surface mode, as its spectral position is invariant with d for a constant n. Examination of the *E*-field distribution along the exit surface revealed that the excitation is highly localized at the corners of the "peninsula" of the C-shape aperture, with a spatial distribution resembling the corresponding Poynting vectors of Fig. 4(b). It is interesting to note that whenever the wavelength of this mode is close to the FP modes, there occurs a spike in local *E*-field magnitude at point P2, as the inset of Fig. 1(b) demonstrates.

The study of the effect of n on the resonance wavelengths and PT of the aperture was started with the case where a 300-nm thick Ag film containing the aperture is immersed into an infinite slab of a dielectric material. The representative spectrum of the aperture response for n = 1 [top row in Fig. 3(c)] has an ECSP mode (peak A) at ~1.6 μm and the first FP mode (peak B) at 890 nm. There are significant differences between the transmission characteristics

#120095 - $15.00 USD Received 17 Nov 2009; revised 8 Dec 2009; accepted 10 Dec 2009; published 14 Dec 2009

of the two peaks; the intent to highlight these differences motivates our choice of the Ag layer thickness (300 nm), whereas only 100 nm or so would be sufficient for optical opacity.

In the immersed aperture case, the positions of both peaks A and B scale linearly with n [Fig. 3(a)], matching the analytical expression for a perfect electric conductor [18]. The PT follows a similar trend for both maxima, as shown in the inset of Fig. 3(a). The degree of the PT increase with n is noteworthy, particularly for the longer wavelength peak, where it shows a nearly four-fold increase as n goes from 1 to 4. It is noted that the data shown in Fig. 3(a) also suggest the increase of PT with resonant wavelength, similar to the findings of Ref. [11], where the wavelength was varied by changing the C-aperture dimensions, while n was kept constant. In that case, the authors defined a "correlation length" that is of the order of the resonant wavelength, such that the photons within this length of the aperture are coupled and are transmitted together. Thus, the longer the wavelength, the greater the correlation length, and consequently, more photons are transmitted.

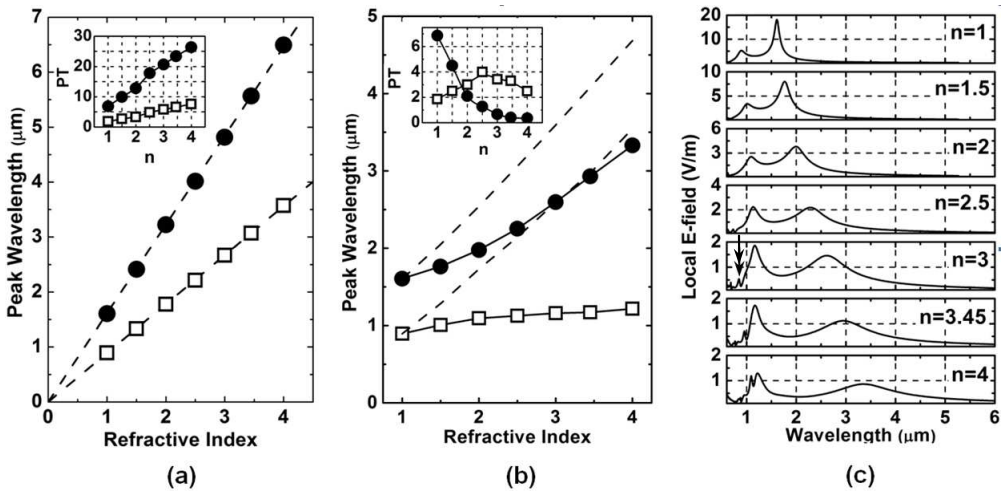

Fig. 3. The shifts of the resonance wavelengths with n in an immersed aperture (a) and the aperture on a substrate (b), at point P1 [cf. Figure 1(a)]. Solid and open symbols represent the data for the ECSP peak [A in Fig. 1(b)] and one of the FP resonances [B in Fig. 1(b)], respectively. The change in resonance wavelength predicted by the analytical model (see text) is shown by the dashed lines. Power throughput at the wavelengths corresponding to the two peaks in spectral response as a function of n is shown in the corresponding insets. (c) Evolution of the spectral E-field response with n for the aperture-on-substrate case. The arrow identifies the peak corresponding to the surface mode D. Note the different abscissa scales for different values of n.

We next examine the case of semi-infinite dielectric layer, i.e., the aperture on a substrate. The results obtained for this configuration are summarized in Figs. 3(b) and 3(c) and differ (in some instances, quite dramatically) from those for the immersed case of Fig. 3(a). While the wavelength of the ECSP peak (solid circles) increases with n, similar to the immersed aperture, the rate of this increase (0.6 μm per unit index) is nearly 3 times lower than that for the immersed case (1.7 μm per unit index). The important finding here is that this dependence is much shallower than expected from the analytical model [18], which predicts a scaling factor of $\sqrt{(n^2+1)/2}$ [shown by the dashed lines in Fig. 3(b)].

The FP peak B [open squares in Fig. 3(b)] is nearly invariant with n. This is again in contrast with the immersed aperture case. Since this peak owes its origin to a FP cavity mode, it is feasible that its position is determined to a large extent by the index of the material filling the cavity (which is vacuum for the aperture-on-substrate configuration). Consequently, the observed modest red-shift can be attributed to the aforementioned phase change upon reflection from the exit surface. PT at this peak increases up to n = 2.5, in a manner similar to

#120095 - $15.00 USD Received 17 Nov 2009; revised 8 Dec 2009; accepted 10 Dec 2009; published 14 Dec 2009

the immersed aperture, but decreases from there on. Closer inspection of the spectral response [Fig. 3(c)] reveals that this decrease is coincidental with the proximity of the surface mode D, which appears as a minor feature at about 0.89 μm for n = 3 and increasingly overlaps the FP peak at higher values of n. Note that while PT for the FP mode exhibits a non-monotonous change, the local E-field decreases steadily with increasing n, as shown in Fig. 3(c). Similarly, referring back to the inset of Fig. 1(b), it can be observed that while the interaction of the FP and surface modes results in the substantial enhancement of local E-field, the forward PT does not necessarily follow the same trend. While the former determines to local intensity, the latter measures the amount of forward power flow and is related to aperture transmittance. This lack of correspondence between the two quantities indicates that high intensity enhancements at the exit surface of the aperture are not necessarily an indicator of aperture transmittance even under near-field conditions.

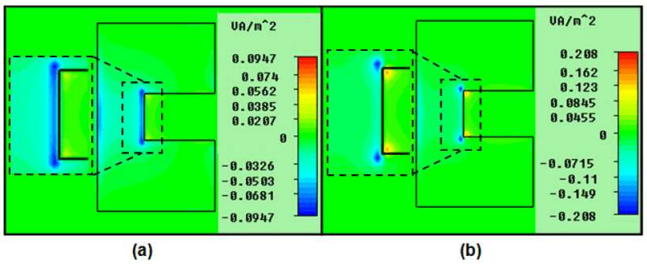

Fig. 4. Spatial distribution of the normal component of the Poynting vector at the exit surface of the Ag film, at the wavelengths of (a) 1.14 μm for n = 2.5 and (b) 1.22 μm for n = 4. Negative sign corresponds to the Poynting vector component along the propagation direction of the exciting wave.

The PT reduction with increased degree of mode overlap is likely due to the change in the spatial distribution of the Poynting vector. This change is evident in Figs. 4(a) and 4(b), where the exit Poynting vector distributions for n = 2.5 and 4 are compared. The interaction of the surface and FP modes at n = 4 [Fig. 4(b)] alters the power flow through the aperture quite dramatically. As is evident from Fig. 4(b), the Poynting vector distribution at the wavelength of the FP mode acquires the symmetry characteristics of the surface mode D, with a large fraction of power being backscattered at the corners of the peninsula of the C-shape. As a result, while the power flow along the sidewall of the aperture is still increasing with n, the net power arriving at the exit surface is diminished. Similar mode interconversion was reported in Ref [22]. and was also attributed to the coupling of the surface and FP modes.

4. Summary

It is shown that the optical properties of a plasmonic aperture are strongly affected by the surrounding medium. For both immersed and on-substrate configurations, the resonant wavelengths increase with n (although to a varying extent). The power throughput behavior is more complicated and is affected not only by the adjacent material, but also, for the aperture-on-substrate configuration, may increase or decrease with n, depending on the interplay of the transmission mechanisms. This work highlights the richness of the optical phenomena involved in subwavelength aperture transmission and demonstrates the importance of accounting for the effect of the surrounding medium when designing such plasmonic devices.

Acknowledgements

This work was partially supported by the NASA Florida Space Grant Consortium under award number: 16296041-Y5.

#120095 - $15.00 USD Received 17 Nov 2009; revised 8 Dec 2009; accepted 10 Dec 2009; published 14 Dec 2009